Nat Hazards (2015) 77:255–272
DOI 10.1007/s11069-015-1600-6

ORIGINAL PAPER

Estimating flooding extent at high return period for ungauged braided systems using remote sensing: a case study of Cuvelai Basin, Angola

A. G. Awadallah · D. Tabet

Received: 3 August 2014 / Accepted: 3 January 2015 / Published online: 18 January 2015

Abstract Floods are the most expensive natural hazard experienced in many places in the world. The current study aimed at estimating the flooding extent at high return periods in the Cuvelai Basin, southern Angola, where no flow, rainfall or accurate topographic data are available. The flooding study thus relies on remote sensing information: archival optical satellite images, data retrieved from the global flood detection system (GFDS) and Tropical Rainfall Measurement Mission data to help characterize flooding events and determine their extents for high return periods, well beyond the available remote sensing record. Landsat and Earth Observing-1 Mission satellite images are used as optical images. The GFDS provides a monitoring of ongoing flood events everyday. Comparison revealed that the GFDS values in the wetland areas are always less than the other satellite flooding extent by about 25 km^2. Frequency analysis was undertaken on the annual maxima flooded areas for monitored GFDS locations using Gumbel distribution. The frequency analysis shows that the potential inundation areas for the 100-year flood event increase by 25 % (±5 %) more than the 10-year event. The remote sensing for the 2009 Landsat image is used to get approximately the flooded areas for the 10-year return period for the whole basin. To assess flooding areas for higher return periods such as the 100-year event, the flooded areas are increased based on the frequency analysis ratio results to give the 100-year inundation extents. Interpolation is undertaken for areas where no data are available from the GFDS website. The Cuvelai Basin inundation areas are thus estimated for non-recorded flooding events.

A. G. Awadallah (✉)
Faculty of Engineering, Fayoum University, Al Fayoum, Egypt

A. G. Awadallah
Dar Al-Handasah, Shair and Partners, Consulting Firm, Cairo, Egypt
e-mail: aawadallah@darcairo.com

D. Tabet
Dar Al-Handasah, Shair and Partners, Consulting Firm, Beirut, Lebanon

Keywords Floods · Remote sensing · Flood frequency analysis · Flooding extent · Cuvelai Basin · Angola

1 Introduction

Floods are the most expensive natural hazard experienced in many places in the world (BTE 2001). Flood behavior and therefore hazard is influenced by a range of factors that vary significantly with location and need to be understood and managed locally (National Flood Risk Advisory Group 2008).

The study area is the Cuvelai Basin (CB) in southern Angola, northern Namibia (Africa). Large flood variations, coupled with a poor record of past floods, provide a significant barrier to understanding the flows and floods of the CB as well as to their sustainable management. Typical data requirements for state-of-the-art flood inundation models require mainly topographic data of the channel and floodplain to act as model bathymetry and time series data of flow rates/stage data to provide model input and output boundary conditions or at least rainfall data with calibrated rainfall/runoff models to compensate for lack of flow data.

For rural floodplain modeling, modelers require that the digital terrain model has vertical accuracy of about 0.5 m and a spatial resolution of at least 10 m. Important exceptions are features such as embankments and levees controlling overbank flow, for which a higher accuracy and spatial scale are required ($\sim$10 cm vertical accuracy and 2 m spatial resolution) (Smith et al. 2006).

Flood inundation models require also discharge and/or stage data to provide model boundary conditions. The data are usually acquired from gauging stations spaced 10–60 km apart on the river network. Hydrologic and hydraulic data are needed for braided streams, since in the case of the CB, hydrologic and hydraulic modeling is extremely extensive. Unfortunately, the quantity and quality of data available for the CB for use in analyzing flood events are very poor. Overall, there are specific weaknesses in respect of:

- Available topographic mapping is largely planimetric in content. Vertical scale is insufficient for flood planning across entire basin. Topographic data rely mainly on Shuttle Radar Topography Mission with 90-m resolution at ground.
- No records available on flood frequency, flow height, frequency and duration for any channel. Where records or reports are available, they are incomplete and often anecdotal and unsubstantiated.
- Few historical data derived from secondary sources are present in the literature on rainfall intensity, frequency and distribution throughout the year in and around Ondjiva (the main city of the CB).
- Data on discharge, runoff coefficients, and evapotranspiration rates for natural or planted systems within the CB and empirical analysis of the relationships to define runoff rates are not available.

In this context, we have not been able to "model" the flood. Instead, we have sought to characterize and understand it and estimate its extent at high return periods in order that appropriate measures may be considered in planning for it. In the absence of meaningful, directly obtained data sets, we have relied on available satellite imagery as the primary source of data, supported by a limited range of other, secondary data.

We present in this paper the methodology and results aiming at proposing flood protection schemes for population centers in the CB. The structure of the paper is as follows. After this introduction, we present a brief account of the CB, focusing on the Angolan side of the basin (Sect. 2). Then, we describe the available data, followed by the methodology undertaken to overcome data limitations (Sect. 3). The results are presented and analyzed in Sect. 4, followed by the study conclusions in Sect. 5.

2 Study area

The CB covers an area between the Cubango and Cunene rivers, as shown in Fig. 1, and it is shared between Angola and Namibia with an approximate area of 170,000 km^2, <40 % is located in Angola and the rest in Namibia. The Angolan part of the CB is home to around 400,000 people, while the Namibian part is home to about 800,000 capita (Mendelsohn and Weber 2011). The Angolan part of the CB is stretching across two provinces, namely Cunene and Cuando–Cubango. The Basin is situated in a flat landscape at approximately 1,100 m above sea level. Soils consist of clayey sands in the lower parts of the landscape and sands on surrounding relatively higher ground. The basin is made up of a network of interconnected water channels originating in the highlands of central Angola, flowing southward into Namibia and spreading across the low-lying, gently sloping areas of the Kalahari sands into the Etosha Pan at its southern reaches. This drainage system is an important river system characterized by a number of shallow ephemeral watercourses covering an area of about 7,000 km^2 of ephemeral channels. The interconnected network of channels acts as a pathway for flooding that recharges groundwater aquifers in the basin. Groundwater recharge is one of the most important functions of floods: As water travels down the channels, it infiltrates into the sandy and gravel alluvial deposits of the channel beds.

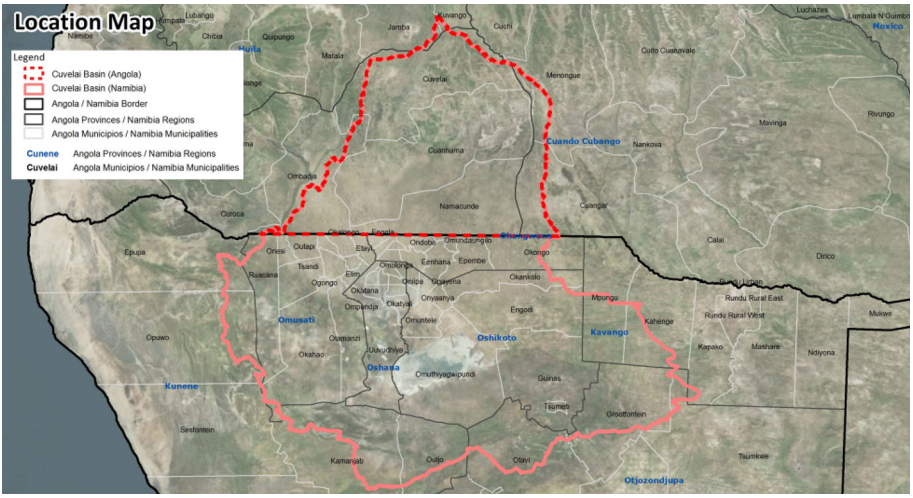

Fig. 1 Location map of the Cuvelai Basin

The climate is semiarid, and the area receives an average annual precipitation of approximately 300 mm in the southwest, while the northeastern part of the basin belongs to a tropical climate. Rainfall is highly variable in time and space.

There is only one significant urban area, Ondjiva, within the CB, and one main corridor of development from Cuvelai to the Namibian border, along the north–south highway. Development is most intense between the border and Ondjiva though even here it remains sparse with population densities of <20 persons per sq. km. North of Ondjiva development is much less intensive.

Larger scale, damaging floods are not uncommon, and these cause significant hardship to the population, most recently in 2008, 2009, 2010 and 2011 (DREF 2009, 2010, 2012). Historically, there has been little intervention in respect of flood management. The emphasis has been on passive management, such as locating residential and other critical assets on land known not to flood.

3 Data available and methodology

The available remote sensing data can be categorized into four types: (a) archival optical satellite images, (b) global flood detection system data, (c) Tropical Rainfall Measurement Mission and (d) Shuttle Radar Topography Mission.

3.1 Optical satellite images

Detection of inundation on optical satellite images is possible because of the low reflectance of the water bodies, which make them easy to detect. However, the major difficulty is to find cloud-free images during the flood events, or as close as possible from the flood event. Flooding detection in this study was based on Landsat and EO-1 images.

The Landsat program is the longest running enterprise for acquisition of satellite imagery of Earth. Landsat 7 launched in 1999 is still functioning, but with a faulty scan line corrector since May, 2003. Therefore, all images retrieved had wedge-shaped gaps (regular missing/bad lines) on both sides of each scene, resulting in approximately 22 % data loss. The temporal resolution of Landsat 7 images is 16 days. The main instrument on board Landsat 7 is the enhanced thematic mapper plus, which provides one panchromatic

Table 1 List of optical satellite imageries used for the flood study

Imagery	Imagery type	Dates acquired	Notes
Landsat TM	Optical image	16/04/2004	
Landsat TM	Optical image	26/03/2008	
Landsat TM	Optical image	21/03/2009	
Landsat TM	Optical image	09/04/2010	
Landsat TM	Optical image	28/04/2011	
EO-1 (NASA)	Optical image	30/03/2011	Partial coverage
EO-1 (NASA)	Optical image	03/05/2011	Partial coverage
EO-1 (NASA)	Optical image	13/05/2010	Partial coverage
EO-1(NASA)	Optical image	10/04/2010	Partial coverage
EO-1(NASA)	Optical image	23/04/2010	Partial coverage
EO-1(NASA)	Optical image	16/05/2011	Partial coverage

band (band 8) of a resolution 15 m. Several images acquired during the flood events were downloaded and studied, and they are listed in Table 1.

The Earth Observing-1 Mission (EO-1) satellite is part of NASA's New Millennium Program (NMP) to develop and validate a number of instrument and spacecraft bus breakthrough technologies designed to enable the development of future earth imaging observatories. It was launched in 2000 for 1-year mission, but the expectation of its functioning time has been greatly exceeded. The resolution of the images is 30 m as for Landsat images. Images acquired over particular areas facing environmental problems such as floods are archived and placed in the public domain. The advanced land imager images are of particular interest for the flood study.

Image classification is essential to determine the flooding extent. The Landsat image classification leans on a semiautomated approach that consists of using the first automatic classification (unsupervised classification) to extract the class of water which can be separated from other classes visible in the image. Due to the failure of the scan line corrector and the data loss, a gap-filled algorithm method has been developed and executed in Erdas Imagine software to approximately fill the wedge-shaped gaps with minimum distortion. The filtering technique consists of assigning the majority class within a window of 13 × 13 pixels. The flood class was extracted from the unsupervised classification imagery, converted into polygons, superimposed on top of the Landsat imageries and manually edited by adjusting feature by feature the wrong geometries and digitizing the missing areas.

3.2 Global flood detection system (GFDS) data

GFDS is a space-based river gauging and flood monitoring system, a methodology developed at Dartmouth flood observatory modified at the Joint Research Centre of the European Commission and implemented on an automatic operational basis (Kugler and De Groeve 2007). The technique uses passive microwave data of two satellites (AMSR-E and TRMM), which are sensitive to water surface changes. The sensor revisits every place on

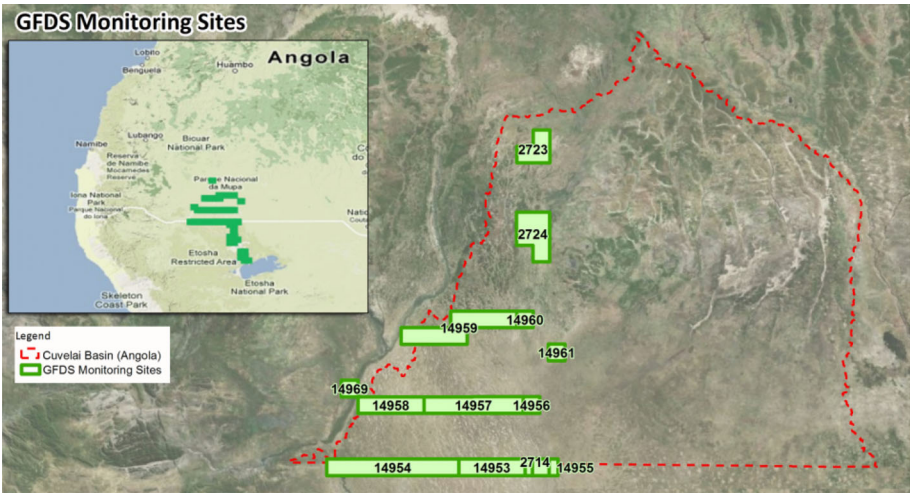

Fig. 2 GFDS monitoring areas in Cuvelai Basin between Angola and Namibia

Earth once per day and can therefore provide a daily temporal resolution (De Groeve and Riva 2009). Thresholding the signal of water surface change allows the detection of riverine inundation events. GFDS provides an alternative to in situ gauging stations in remote areas with accurate time series of flood surface variations. In collaboration with national governments, including Namibia, Haiti and Brazil, GFDS is being integrated within operations of flood forecasting centers and international aid organizations. Among the monitored basins is the CB, monitored in 13 locations in Angola as shown in Fig. 2 (GFDS 2014). It is possible to detect inundation change of a river site in a sub-pixel dimension since most of the observed river channels are not as wide as the observation footprint. To monitor flood events, the brightness temperature values for a number of observation sites over selected river sites were extracted from the AMSR-E satellite images. During a flood event—where water goes over bank—the increased water surface of the inundated area will cause a decrease in the brightness temperature value detected by the satellite (Brakenridge et al. 2007). The 13 areas monitored in Cuvelai are shown in Fig. 2. At each area, the flooding extent can be retrieved for the available captured imageries.

3.3 Rainfall information

Tropical Rain Measurement Mission (TRMM) was used to obtain rainfall information. The TRMM mission was launched on November 1997. TRMM provides systematic, multi-year measurements of rainfall in the tropics as key inputs to weather and climate research. The satellite carries a precipitation radar (PR), a 9-channel passive TRMM Microwave Imager (TMI) and a Visible–Infrared Scanner (VIRS). Besides these three primary payloads, TRMM has two other instruments, the clouds and the Earth's radiant energy system, and the lightning imaging sensor. PR, TMI and VIRS are designed to obtain rainfall and other relevant information such as rain type, height of the bright band, cloud type and cloud top height individually and complement each other's functions. The satellite observations are complemented by ground radar and rain gauge measurements to frequently validate the satellite rain estimation techniques. The product of the TRMM rainfall estimate that was used in this research is the version 7 calibrated by ground radar and rain gauge measurements, usually termed TMPA version 7.

TRMM data cover almost the whole planet, and the estimates are provided on a global $0.25° \times 0.25°$ grid over the latitude band 50°N–S within about 7 h of observation time. The data are available in hourly, daily and monthly formats (NASA 1999) from 1998 to date. Several studies have compared the TRMM data with ground station data, throughout the world and particularly in Africa (Adjei et al. 2012; Haile et al. 2011, 2009; Hughes 2006; Li et al. 2009; Nicholson 2005). Other studies used the TRMM in Angola to derive intensity–duration–frequency curves (Awadallah et al. 2011; Awadallah and Awadallah 2013).

3.4 Topographic information

Topography was analyzed based on two types of data:

- Topographic maps from IGCA (Instituto de Geodesia e Cartografia de Angola) scale 1/100,000, edited in 1982. All maps except one were acquired from IGCA. They were scanned, geo-referenced, clipped and mosaicked.
- Shuttle Radar Topography Mission (SRTM) data with 90-m resolution at ground.

3.5 Methodology

Given the above, the approach proposed does not follow a single flood assessment methodology. It is a composite approach that adapts and applies a number of different techniques and as necessary uses professional judgment to compare the findings with what may be expected, based on similar contexts elsewhere. Unfortunately, none of the analysis carried out could be validated by measured records, due to lack of data. The undertaken methodology is summarized in the following steps and illustrated in Fig. 3:

a. Data collection of available remote sensing data and image classification of satellite imageries and comparison of different sources of flood extent data
b. Characterization of flooding events
c. Frequency analysis of GFDS flooding extents
d. Estimation of flooding extent at high return periods

The above steps are detailed hereafter. Since calibration data are unfortunately not available, the first step in the methodology is to compare the remote sensing information sources, in order to reach a robust and realistic estimate of the flooding extent. The advantages of optical satellite images (Landsat and EO-1) are their good resolution and their well-acknowledged capabilities in landuse determination including water bodies. However, they are available on daily basis and they are very sensitive to cloud coverage, which is unfortunately very common during flooding events. On the other hand, GFDS information relies on passive microwave data (less sensitive to clouds) and is available on daily basis. Thus, it has a higher probability of capturing the maximum daily flooding event. Unfortunately, as will be explained in the results section (Sect. 4a), the flooding extent (in km^2) is not correct as an absolute value (compared to the optical satellite imageries). This might be due to a bias in the calibration of the microwave signal.

The second step in the methodology is to achieve an understanding of the flooding event in the CB. In order to understand flood events in a certain watershed/river system, one has to assess the following:

- Number of flooding events/year
- Time lag of flood, i.e., the time elapsed between the onset of the rainfall and the peak of flood
- Flood magnitude changes over time

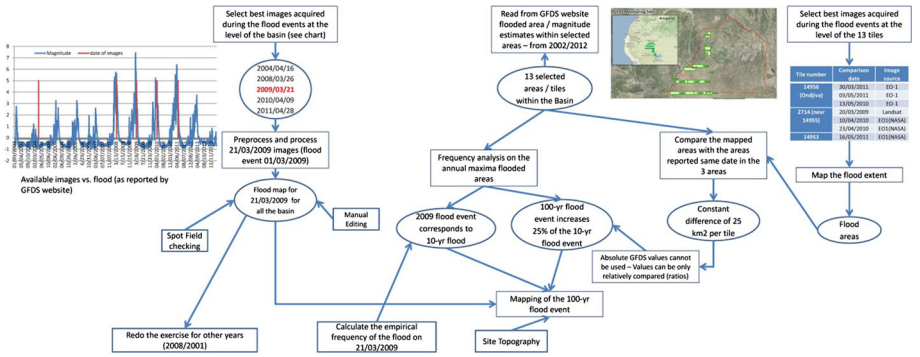

Fig. 3 Illustrative summary of the study methodology

- Flood duration, hydrograph rising time, hydrograph recession time, …
- Flood "speed," i.e., wave advance celerity from one location to another along the breaded stream system.

The above-mentioned characteristics of the Cuvelai floods on the Angolan side of the basin are described in Sect. 4b using the above-mentioned remote sensing information.

The third step in the methodology is to extrapolate the recorded flooding extents to the rare "design" flooding extents (such as the 100-year flooding extent) to achieve a high standard of protection. This is undertaken using frequency analysis. Frequency analysis is a statistical procedure that aims to estimate the probability of occurrence of rare events, based on the information of past events, considered representative of the studied process. This estimation is based on the definition and fitting of a frequency distribution, which is an equation describing the statistical behavior of the collected data, in this case, the maximum annual flooding extent data. First, the maximum value for daily flooding extent was determined for each of the 10 years of available data, resulting in ten values, one for each year. Several frequency distributions are tested to select the most "appropriate" one to fit the data. To choose between potential distributions, the visual fitting comparison might be subjective and misleading. To remedy this subjectivity, one can use one of many approaches: among them the moment ratio diagrams, the methodology proposed by El Adlouni et al. (2008) and/or the use of Akaike and Bayesian information criteria. The last two features are available in Hyfran software (INRS 2008). Based on the three approaches listed above, and following the parsimony principle which favors using distributions with fewer parameters, the Gumbel distribution was selected to fit the GFDS maximum annual flooding extent data. For each GFDS location, the Gumbel distribution is fitted using the method of moments. The Gumbel equation allows extrapolating the data beyond the 10-year extent to estimate the flooding corresponding to the 25, 50 and 100 years, and the previously mentioned ratios between these flooding extents and the 10-year base case flooding extent are determined. The results of the above procedure are shown in Sect. 4c.

Although the GFDS data are not accurate as absolute values, we assumed in this research that their values relative to each others are correct. This allows performing a

Fig. 4 Flooding extent near Ondjiva depicted from EO-1 and Landsat imageries of the March 30, 2011

frequency analysis on the GFDS maximum daily flood extent data to estimate the ratios between the 100-year flooding extent and the baseline 10-year flooding extent. The later 10-year flooding extent is determined using the optical satellite imageries and not the GFDS to remedy for the GFDS underestimation of flooding.

4 Results

4.1 Flood extent comparison

First the Landsat and the EO-1 were compared and found quasi-identical as shown for the 30/3/2011 imagery of the flood event just as an example: Fig. 4 shows the flooding extent near Ondjiva city depicted from cloud-free Landsat and EO-1 images acquired after the flood events. The detection of flood from an optical satellite image is possible due to the low reflectance of the water bodies, which make them easy to detect. This leans on a semiautomated approach that consists of using the first automatic classification (unsupervised classification) to extract the class of water in blue (foreground image), which can be separated from other classes visible in the image.

In the next step, a comparison was made between the values downloaded from the GFDS website (GFDS 2014) (in different days, spanning several years) with the extent of water spread as detected from EO-1 (NASA) and Landsat imageries. The results revealed also that the GFDS values in the wetland areas (as it is the case near Ondjiva, Cuvelai, area 14,956, 100 km^2) are always less than the other satellite flooding extents by a constant amount of about 25 km^2. Other regions were also tested, and they yielded similar constant differences. Although one would have expected the difference between the two flooding extent estimates to be proportional to the inundated area or to the monitoring area, the empirical finding of constant difference may suggest a bias (constant error) in the GFDS calibration that appears in the estimate of the flooding areas in the Angolan side of the CB. In any case, the issue is not important since the extent of the optical satellite imageries is the one adopted in further analysis. Table 2 shows the comparison of the inundated areas in each event versus the GFDS flooded areas.

Table 2 Flood extent comparison between the EO-1 (NASA), Landsat imageries and the global flood detection system (GFDS) data

Tile number	Comparison date	Image source	Inundated area (km^2) based on:		Difference between satellite and GFDS extents
			GFDS	Satellite images	
14956 (Ondjiva)	30/03/2011	EO-1(NASA)	21.00	47.04	26.04
	03/05/2011	EO-1(NASA)	9.48	36.32	26.84
	13/05/2010	EO-1(NASA)	5.74	30.58	24.84
2714 (near 14955)	20/03/2009	Landsat	22.61	48.38	25.77
	10/04/2010	EO-1(NASA)	15.00	38.74	23.74
	23/04/2010	EO-1(NASA)	19.36	43.88	24.52
14953	16/05/2011	EO-1(NASA)	21.93	48.11	26.18

The above finding indicate that we may rely on the GFDS data to undertake a frequency analysis on the 10 years of available flooding data, but the flooding data cannot be considered in their absolute values. On the other hand, the 2009 flooding event resulted in widespread impacts and is extensively covered by useable satellite imagery. It is also the largest flood event over the last 10 years and thus may be taken to be representative of the 1 in 10-year event. Therefore, it is used as the base year for much of the additional analysis. The extent of floods on March 21, 2009, is presented in Fig. 5, which shows the flooding percentage coverage depicted from the event dated March 21, 2009. The whole Angolan side of the CB is divided into equal "squares". For each square of the image, the percentage of flooded lands is calculated with respect to the total area of the square. The flooding percentages are classified into eight classes ranging from green (minimum flooding) to dark orange and red (maximum flooding), while the gray color indicates no flooding. The squares in pink represent the area in Ondjiva already protected by dikes. Flood areas in this image cover some 4,150 km^2 in area, approximately 7.6 % of the Basin.

4.2 Characterization of flood events

As shown in Fig. 6, illustrating flood magnitude as per GFDS data, there are numerous flood events and peaks in a typical year. In this case, the annual extent refers to the maximum extent of a single flood event in that year.

The time lag of a flood is defined as the time between the onset of a rainfall event and the start of flooding. In the absence of rainfall and runoff data, the satellite rainfall data from the TRMM and the GFDS flood magnitude values were utilized to estimate flooding lag time.

Although the accuracy of the TRMM data for the CB cannot be confirmed, it can be concluded that it correctly replicates the seasonal distribution of rainfall. Going further, the available years of TRMM data (from 2001 to 2011) show an annual average rainfall of 910 mm in the lower Basin some 50 % higher than the long-term average shown on the isoheytal map. This could be due to a simple bias in TRMM data (higher estimates than observed rainfall) or equally it may be that rainfall in the 10 years of data was exceptionally high.

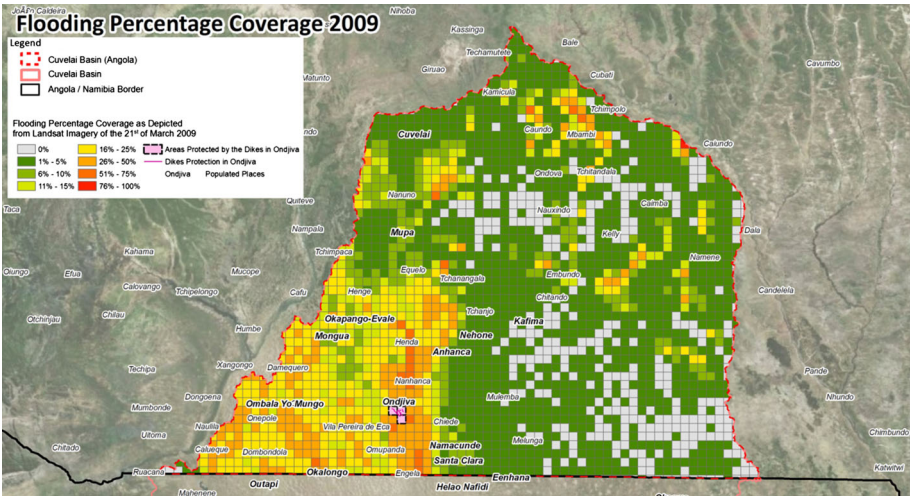

Fig. 5 Flooding percentage coverage as depicted from Landsat imagery

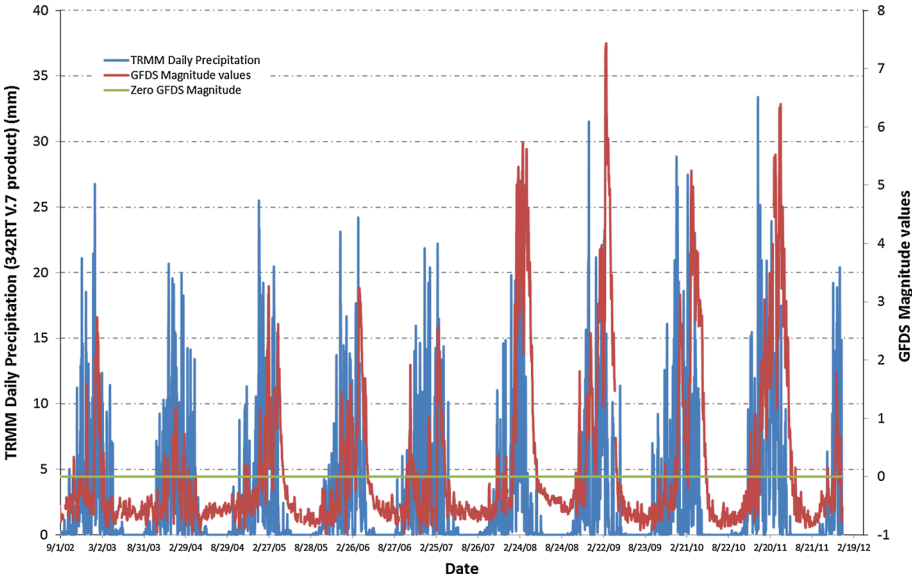

Fig. 6 Flood magnitude peaks (as reported by GFDS) within the CB

The latter case (i.e., rainfall in the 10 years of available data was exceptionally high) is consistent with the analysis of floods prepared by Mendelsohn and Weber (2011) reproduced in Fig. 7. This figure shows the magnitude of flooding from 1941 till 2011.

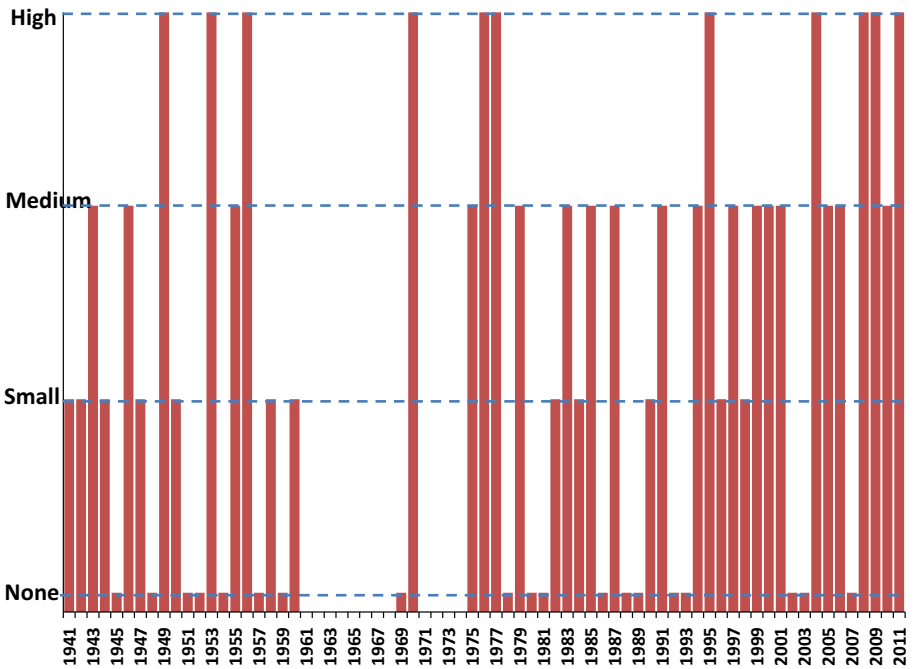

Fig. 7 Inter-annual variation of flooding in Cuvelai Basin (after Mendelsohn and Weber 2011)

Floods are categorized as: high, medium, small floods and no floods. In the Mendelsohn and Weber (2011) study period spanning 71 years (which includes 13 years for which no information is available), exceptionally high flows occurred eleven (11) times: in 1949, 1953, 1956, 1970, 1976, 1977, 1995, 2004, 2008, 2009 and 2011. There were no or only negligible flows in 19 years, giving a frequency of high flows slightly <20 % (i.e., 1 every 5 years). No or negligible flow were more common occurring every 1 in 3.1 years.

Comparing long-term (full period, 69 years) and short-term records (since 2001) shows a much higher frequency in the recent past, with 4 years of exceptionally high flows in the last 10 years, i.e., double the long-term frequency depicted in the Mendelsohn and Weber's (2011) analysis.

GFDS data for Evale and Ondjiva provide flood magnitude data. The elapse time difference between the peak floods in Evale and Ondjiva is in the order of 5–7 days in 4 out of 9 years and 12–14 days in 3 out of 9 years. The average time for the flood wave advance is 9 days with a minimum of 5 days. The comparison of the TRMM and GFDS data on a daily basis is also shown in Fig. 6. These data are consistent with Mendelsohn and Weber (2011) for the 2009 flood, which showed that the flood waters travelled a distance of 67 km (between Evale and Ondjiva) in 4 days (i.e., with a speed of approximately 16–17 km/day).

It is noted that the maximum flood magnitude is delayed compared with the beginning of the rainy season and even compared with the high rainfall values at the beginning of the rainy season. This indicates that an accumulation of rainfall is required before a flood event occurs.

If it is accepted that any flow in an ephemeral channel comprises a flood, the following can be noted:

- The duration of flooding ranges from 1 month up to more than 5.5 months (in the 2011 extreme flood event), with an average of 3.24 months.
- The time between the peak flood and full recession of the flood ranges from 1 week to greater than 2 months and averages 1.4 months. This flood recession is 30–40 % of the total flood time indicating that the rising limb is longer than the recession limb. This would be atypical of most flood events. For typical "channel" type of floods, the recession limb is around 1.67 times the rising limb further reflecting on the slow speed of water advance.
- If the magnitude reported by the GFDS website is considered as a measure of the "severity" of the flood, two measures of magnitude can be calculated: the maximum magnitude during 1 year and the average magnitude during 1 year. Plotting these two measures on the same graph (Fig. 8) shows that the highest peak magnitude is in 2009, while the highest average magnitude is in 2008. It should be noted that no deaths were reported in the 2008 event, while deaths were reported, especially in Evale and Ondjiva in the 2009 floods. It appears that death occurrence is more linked to the peak flood magnitude and not to the average magnitude.

Depending on how the severity of a flooding event is defined the 3 years of 2008 (the highest average flood magnitude), 2009 (the highest peak flood magnitude) and 2011 (the longest flooding duration) may all be considered years of extreme flooding at Ondjiva.

4.3 Flood frequency analysis of GFDS data

Using Gumbel distribution, frequency analysis was undertaken on the annual maxima of flooded area for all 13 locations of GFDS data to deduce the ratio between the rare events

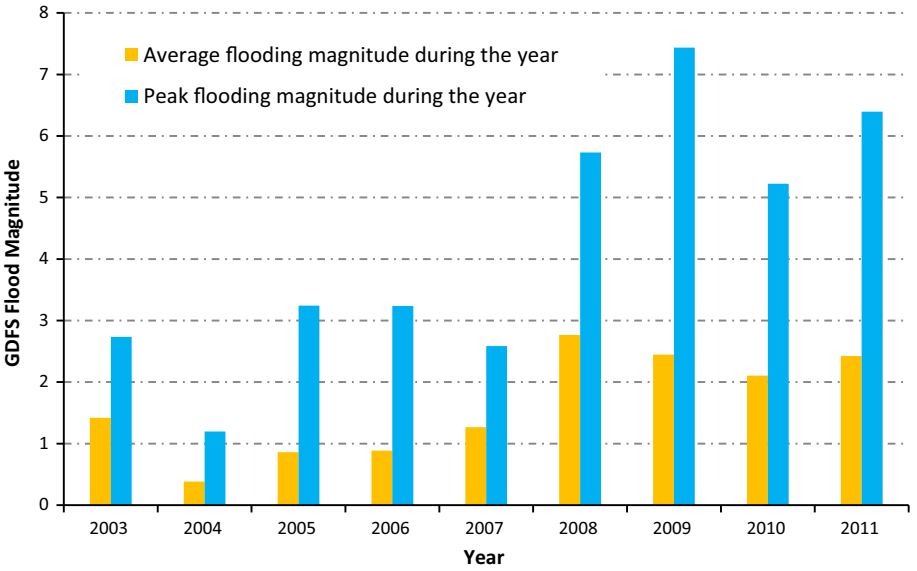

Fig. 8 GFDS flood magnitude peak and average values in the Ondjiva area

(1:10 and 1:100 years, for example). To avoid the error depicted in the GFDS data, only the ratio between the return periods is utilized and not the area of flood extent itself. This ratio will be then multiplied by the wet (flooding) extent as detected from the optical EO-1 and Landsat imageries. This procedure gets around the discrepancy between the GFDS and the other satellites defined water spread.

The Gumbel two-parameter distribution method was found to best fit the available GFDS data and is widely used in hydrologic studies. In cases where data are weak, a two-parameter distribution is considered more robust than the three-parameter approach traditionally applied, to avoid over-fitting in limited data. The flood extent fittings are shown in Fig. 9 and Table 3. Each of the figures shows the Gumbel fitting (middle red line) and the 95 % confidence interval of the quantile estimate (blue lines). The value of the 100-year flooding extent is the one corresponding to 0.99 probability, i.e., on Fig. 9a, for example (GFDS location 14969), the 100-year extent is 23 km^2 with a confidence interval ranging from 14.2 to 31.9 km^2.

The frequency analysis shows that the potential inundation areas for the 100-year flood event are 25 % (±5 %) greater than for the 10-year event. A direct relationship developed between the buffer distance from the 10-year extent and the area increase for each flood polygon gives the buffer distance to apply to increase the area of 25 %.

It should be noted that the frequency analysis is undertaken on the flooding extent and not on the flooding depth. This is atypical, but is suited to the CB with its very low relief and flat topography. Interpolation is undertaken for areas where no data are available from the GFDS website.

4.4 Determination of flood extent for high return periods

The 2009 Landsat images are used to get approximately the flooded areas for the 10-year return period for the whole basin. The class of water detected from Landsat imageries

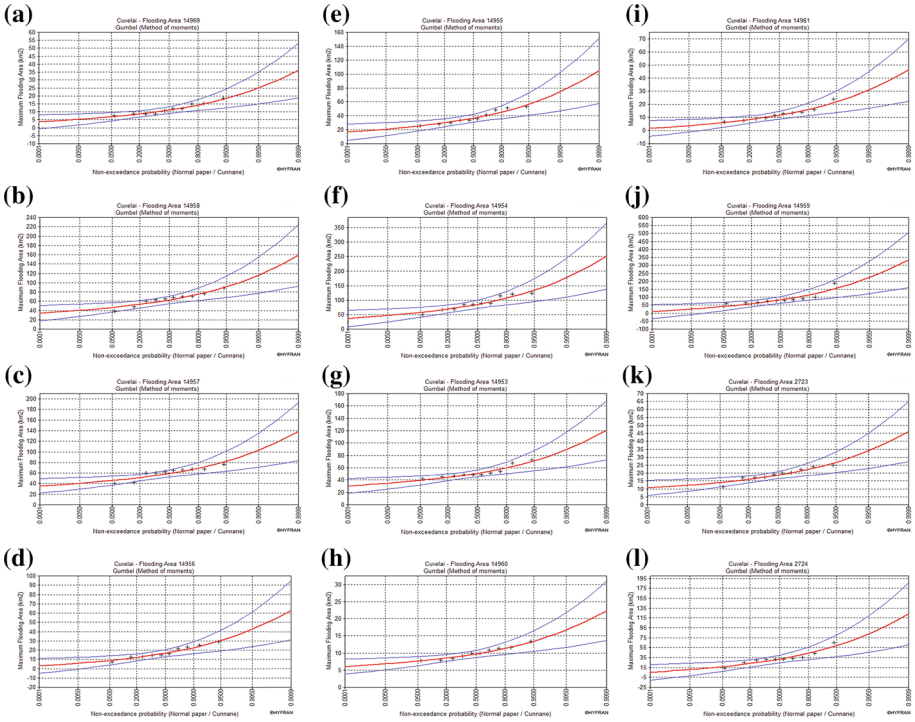

Fig. 9 Gumbel GFDS flooding area frequency analyses

dated 2009 was automatically extracted using the remote sensing techniques. The output was converted into polygons and then superimposed on top of the Landsat imageries where manual editing procedures were applied on the features to adjust the wrong geometries and digitize the missing areas. The final output is shown in Figs. 10 and 11.

Since the GFDS data span only 10 years, the highest reported event (of 2009) is considered empirically as a 1 in 10-year event or higher, based on empirical evidence as it is the higher recorded in a 10-year span of data. If we have assumed this event to be of 50-year return period, for example, the ratios between the 100-year and the 50-year events are lower than the ratios between the 100-year and the 10-year events. Thus, the same extent of the 2009 event would have been multiplied by a smaller ratio to get the 100-year flooding extent. Consequently, since the ultimate goal is to provide schemes for flood protection for the CB populations, the 2009 event was assumed to be corresponding to the lower possible return period to be on the conservative side.

To assess flooding areas for higher return periods such as the 100-year event, the flooded areas are increased based on the frequency analysis ratio results to give the 100-year inundation extents. Based on the previously described methodology, the CB inundation areas are thus estimated for non-recorded flooding events using the above-mentioned stratagem. Interpolation is undertaken for areas where no data are available from the GFDS website.

Figure 11 previews six-sample blow-up areas showing the flooding areas depicted from 2009 Landsat images over the estimated 100-year event and the potential immersed urban areas after the 100-year event.

Table 3 Flood frequency analysis results for GFDS data and deduced ratios

Flood extent	Tile number												
	14969	14958	14957	14956	14955	14954	14953	14960	14961	14959	2723	2724	2725
100 years (km^2)	23.00	109.0	97.00	38.80	69.20	165.0	84.20	15.70	28.20	203.0	31.80	75.60	59.90
10 years (km^2)	16.40	83.00	75.90	26.50	51.10	121.0	65.70	12.40	19.00	137.0	24.50	51.30	45.90
% increase	28.70	23.85	21.75	31.70	26.16	26.67	21.97	21.02	32.62	32.51	22.96	32.14	23.37

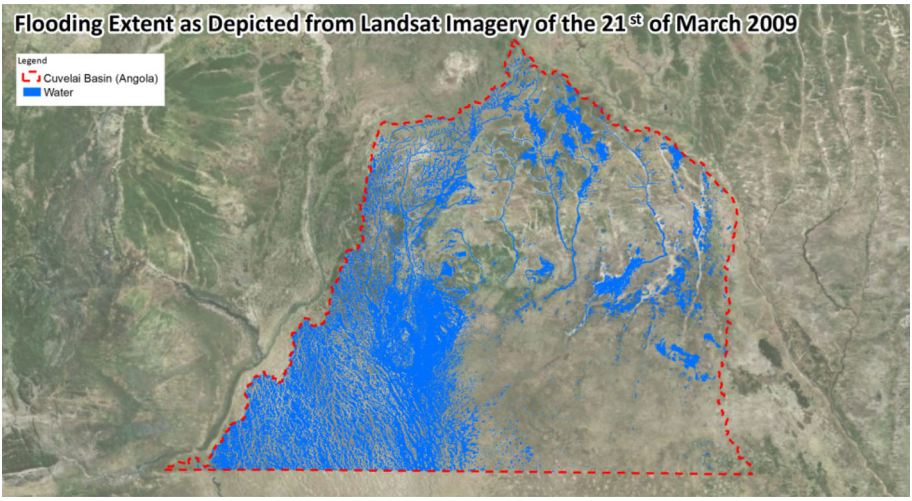

Fig. 10 Flooding extent for 2009 flood as depicted from the Landsat March 2009

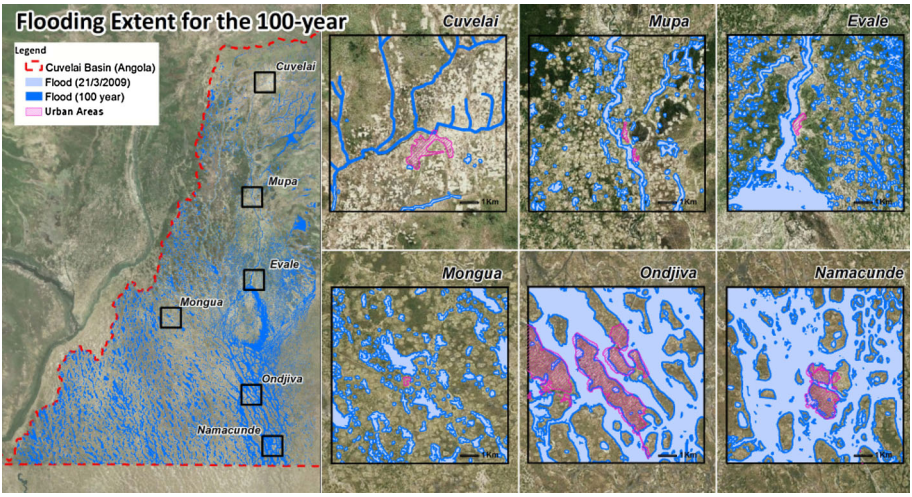

Fig. 11 Flooding extent for the 100-year return period

5 Conclusions

The objective of the current study was to estimate the flooding extent at high return periods in a braided stream context where data of flow, rainfall and topography are lacking. The flooding extent is determined, thanks to remote sensing information: archival optical satellite images, data retrieved from the GFDS and TRMM data. Due to lack of calibration measurements, the methodology relies on comparing sources of remote sensing information and extrapolating beyond the available information.

Landsat and Earth Observing-1 Mission (EO-1) satellite images are used to get approximately the flooded areas for the 10-year return period for the whole basin. They were found to give very similar results. The GFDS provides daily monitoring of

ongoing flood events. Comparison revealed that the GFDS values in the wetland areas are always less than the other satellite water spreads by about 25 km^2. Frequency analysis was undertaken on the annual maxima flooded areas for monitored GFDS locations using Gumbel distribution. The frequency analysis shows that the potential inundation areas for the 100-year flood event increase by 25 % (±5 %) more than the 10-year event.

To assess flooding areas for higher return periods such as the 100-year event, the flooded areas of the 2009 event detected from the optical satellite imageries, considered empirically as a 1 in 10-year event, are increased based on the frequency analysis ratio results (of the GFDS daily data) to give the 100-year inundation extents. The CB inundation areas are thus estimated for non-recorded flooding events, and flood protection schemes could be designed for major cities in Cuvelai.

Acknowledgments This study was undertaken as part of the "Flood Management Study", included in the "Integrated Water Resources Management of Cuvelai Basin" project, awarded to Dar Al-Handasah, Shair and Partners, Consulting Firm. In addition, the authors acknowledge the efforts of F. Nassar, A. El Mofty and M. Sader, GIS specialists, who made enormous inputs to this work and transformed the tedious remote sensing methodology to reality. Also, special thanks to R. Boalch and P. Speight, environmental experts, H. El Badry, Principal, F. El-Khoury, Director, Dar Al-Handasah who reshaped parts of this paper and challenged the authors to overcome the lack of data.

References

Adjei KA, Ren L, Appiah-Adjei EK, Kwabena Kankam-Yeboah K, Anning Agyapong AA (2012) Validation of TRMM data in the black volta basin of Ghana. J Hydrol Eng 17(5):647–654

Awadallah AG, Awadallah NA (2013) A novel approach for the joint use of rainfall monthly and daily ground station data with TRMM data to generate IDF estimates in a poorly gauged arid region. Open J Mod Hydrol 3(1):1–7

Awadallah AG, ElGamal M, ElMostafa M, ElBadry H (2011) Developing intensity-duration-frequency curves in scarce data region: an approach using regional analysis and satellite data. Engineering 3(3):215–226

Brakenridge GR, Nghiem SV, Anderson E, Mic R (2007) Orbital microwave measurement of river discharge and ice status. Water Resour Res 43(4):W04405. doi:10.1029/2006WR005238

BTE (2001) Economic costs of natural disasters in Australia. Report 103, Bureau of Transport Economics, Canberra

De Groeve T, Riva P (2009) Global real-time detection of major floods using passive microwave remote sensing. In: Proceedings of the 33rd international symposium on remote sensing of environment stress, Italy, May 2009

Disaster Relief Emergency Fund (DREF) (2009) Operation, international federation of red cross and red crescent societies Angola: floods. http://www.ifrc.org/docs/appeals/09/MDRAO003.pdf

Disaster Relief Emergency Fund (DREF) (2010) Angola floods; Operation MDRAO003. http://reliefweb.int/sites/reliefweb.int/files/resources/AB12EA6D6127AA22C125770D0040DDEE-Full_Report.pdf

Disaster Relief Emergency Fund (DREF) (2012) http://www.ifrc.org/docs/appeals/annual11/MAA0001011ar.pdf

El Adlouni S, Bobée B, Ouarda TBMJ (2008) On the tails of extreme event distributions in Hydrology. J Hydrol 355:16–33

Global Flood Detection System (GFDS) (2014) JRC European Commission. http://old.gdacs.org/flooddetection

Haile AT, Rientjes THM, Gieske A, Gebremichael M (2009) Rainfall variability over mountainous and adjacent lake areas: the case of Lake Tana basin at the source of the Blue Nile River. J Appl Meteorol Climatol 48(8):1696–1717

Haile AT, Rientjes T, Habib E, Jetten V (2011) Rain event properties and dimensionless rain event hyetographs at the source of the Blue Nile River. J Hydrol Earth Syst Sci 15:1023–1034. doi:10.5194/hess-15-1023-2011

Hughes DA (2006) Comparison of satellite rainfall data with observations from gauging station networks. J Hydrol 327(2006):399–410

INRS (2008) Guide for the use of the decision support system (DSS) for HYFRAN plus software. Institut National de Recherche Scientifique, Eau, Terre et Environnement, Québec

Kugler Z. De Groeve T (2007) The global flood detection system. Office for official publications of the European communities, EUR 23303 EN

Li L, Hong Y, Wang J, Adler RF, Policelli FS, Habib S, Irwn D, Korme T, Okello L (2009) Evaluation of the real-time TRMM-based multi-satellite precipitation analysis for an operational flood prediction system in Nzoia Basin, Lake Victoria, Africa. Nat Hazards 50(1):109–123

Mendelsohn J, Weber B (2011) The Cuvelai Basin—its water and people in Angola. Development Workshop Angola and RAISON Namibia. http://www.dw.angonet.org/sites/default/files/online_lib_files/CUVELAI%20BASIN%20-%20BACIA%20DO%20CUVELAI.pdf

NASA (1999) TRMM precipitation radar algorithm instructional manual (Version 1)

National Flood Risk Advisory Group (2008) Flood risk management in Australia. Aust J Emerg Manag 23(4):21–27

Nicholson S (2005) On the question of the "recovery" of the rains in the West African Sahel. J Arid Environ 63(3):615–641

Smith MJ, Edwards EP, Priestnall G, Bates PD (2006) Exploitation of new data types to create digital surface models for flood inundation modelling. FRMRC Research report UR3, June 2006. pp 78